Constraining composite Higgs models using LHC data

Avik Banerjee,[a] **Gautam Bhattacharyya,**[a] **Nilanjana Kumar**[a] **and Tirtha Sankar Ray**[b]

[a]*Saha Institute of Nuclear Physics, HBNI,*
1/AF Bidhan Nagar, Kolkata 700064, India

[b]*Department of Physics and Centre for Theoretical Studies,*
Indian Institute of Technology Kharagpur,
Kharagpur 721302, India

E-mail: avik.banerjeesinp@saha.ac.in,
gautam.bhattacharyya@saha.ac.in, nilanjana.kumar@saha.ac.in,
tirthasankar.ray@gmail.com

ABSTRACT: We systematically study the modifications in the couplings of the Higgs boson, when identified as a pseudo Nambu-Goldstone boson of a strong sector, in the light of LHC Run 1 and Run 2 data. For the minimal coset $SO(5)/SO(4)$ of the strong sector, we focus on scenarios where the standard model left- and right-handed fermions (specifically, the top and bottom quarks) are either in **5** or in the symmetric **14** representation of $SO(5)$. Going beyond the minimal $\mathbf{5_L} - \mathbf{5_R}$ representation, to what we call here the 'extended' models, we observe that it is possible to construct more than one invariant in the Yukawa sector. In such models, the Yukawa couplings of the 125 GeV Higgs boson undergo nontrivial modifications. The pattern of such modifications can be encoded in a generic phenomenological Lagrangian which applies to a wide class of such models. We show that the presence of more than one Yukawa invariant allows the gauge and Yukawa coupling modifiers to be decorrelated in the 'extended' models, and this decorrelation leads to a relaxation of the bound on the compositeness scale ($f \geq 640$ GeV at 95% CL, as compared to $f \geq 1$ TeV for the minimal $\mathbf{5_L} - \mathbf{5_R}$ representation model). We also study the Yukawa coupling modifications in the context of the next-to-minimal strong sector coset $SO(6)/SO(5)$ for fermion-embedding up to representations of dimension **20**. While quantifying our observations, we have performed a detailed χ^2 fit using the ATLAS and CMS combined Run 1 and available Run 2 data.

KEYWORDS: Beyond Standard Model, Higgs Physics, Technicolor and Composite Models

ARXIV EPRINT: 1712.07494

Contents

1 Introduction

With increasing precision in measurements of the Higgs boson properties at the Large Hadron Collider (LHC), the possibility that the Higgs may be a composite object [1–5] can be put to stringent tests. In this context, the scenarios where the Higgs is identified as a pseudo Nambu-Goldstone boson (pNGB) of a strongly interacting sector are of special interest. This has received considerable attention following its identification as a holographic dual of 5d gauge-Higgs unification models [6–9]. In this paper, however, we stick to an effective 4d scenario, and do not comment on possible UV completion of such models. The approximate shift-symmetry of the pNGBs can screen the weak scale from physics beyond the compositeness scale ($f \sim \mathcal{O}(\text{TeV})$). This provides a well-motivated framework for natural electroweak symmetry breaking.

The direct signatures of these models at the LHC could be the appearance of additional resonances of the strong sector [10–18]. However taking cue from non-observation of these resonances, attempts have been made to push up the resonance masses while keeping the theory still natural [19–23]. The other inevitable and testable features of these models are deviations of the Higgs couplings compared to their standard model (SM) predictions.

One of the consequences of compositeness is that the couplings are replaced by form factors which are momentum dependent. However, it is difficult to test this momentum dependence at the LHC. Nevertheless, the nonlinearity of the pNGB dynamics provides a finite shift in the Higgs couplings measurable in the precision era of the LHC. In this paper we make a systematic study of the pattern and constraints on such modifications that arise in a general class of composite Higgs models.

We categorize the scenarios considered under three major heads:

- *Minimal model*: coset SO(5)/SO(4), with both the left- and right-handed fermions kept in the fundamental **5** of SO(5), represented in literature as MCHM$_{5_L-5_R}$ [24–29].

- *Extended models*: coset SO(5)/SO(4), with at least one of the left- or right-handed fermions kept in the symmetric **14** of SO(5). They are denoted in literature as MCHM$_{14_L-14_R}$, MCHM$_{14_L-5_R}$, and MCHM$_{5_L-14_R}$ [29–35].

- *Next-to-minimal models*: coset SO(6)/SO(5), denoted as NMCHM, with different choices of representation up to dimension **20** [21, 36–44].

The couplings of the pNGB Higgs with the weak gauge bosons (VVh) are usually suppressed in a general class of composite models. The parameter $\xi \equiv v^2/f^2 \ll 1$, where $v = 246\,\text{GeV}$ is the electroweak vacuum expectation value (vev), controls this suppression. The Yukawa couplings are generated through a mixing between the elementary fermions and the operators of the strong sector. Once the strong sector is integrated out the effective Higgs-fermion interaction term looks like [45, 46],

$$\mathcal{L}_{\text{eff}} \propto \bar{f}_L H f_R \mathcal{F}\left(\frac{H^\dagger H}{f^2}\right) , \tag{1.1}$$

where $\mathcal{F}(H^\dagger H/f^2)$ is a function of the SU(2)$_\text{L}$ doublet Higgs field (H). The contributions from the higher dimensional operators with independent coefficients, added to the SM dimension-4 Yukawa term, give rise to a modification in the couplings of the Higgs with the fermions ($f\bar{f}h$), see also [47, 48] in a different context. In the minimal model, the SM fermions couple to only one operator of the strong sector. As a result the modification of the couplings depends on only one free parameter ξ. The other parameters in the effective Lagrangian are fixed from the requirement of reproducing the corresponding SM fermion mass. Therefore, $f\bar{f}h$ and VVh couplings get highly correlated, and stringent constraints on f emerge [49, 50] from the increasingly precise measurements of Higgs production and decays at LHC. In the extended models, owing to the presence of more than one invariant in the Yukawa sector with different coefficients, the correlation between $f\bar{f}h$ and VVh modifiers is weakened, and we observe a possible relaxation of the bound on f. This happens in certain regions of the parameter space where a possible enhancement in $f\bar{f}h$ vertex can partially offset the suppression in VVh coupling. Additionally, the extended

models, carrying more than one invariant in the Yukawa sector, have the distinct advantage of being free from 'double tuning' [30].[1]

In this paper, we first concentrate on a systematic and comparative study of various possibilities of Higgs coupling modifications in the context of the extended models.[2] For each such possibilities, we construct one-loop Coleman-Weinberg Higgs potential [52], and identify regions of parameters space where the top mass, Higgs mass and the electroweak vev are reproduced. Next we consider the next-to-minimal model which contains a SM scalar-singlet (η) apart from the Higgs doublet. Their mixing can significantly modify the observed Higgs boson couplings. In this context also, we survey different fermionic representations and calculate the corresponding modifications to Yukawa couplings.

We then construct an effective phenomenological Lagrangian whose parameters capture the coupling modifications of a general class of models mentioned earlier. The explicit connection between the coefficients of the Lagrangian and the parameters of the specific models is specified on a case-by-case basis. We perform a χ^2 analysis with the ATLAS and CMS combined Run 1 [53] and available Run 2 data [54–66] to estimate a bound on f in the extended models and compare it with that of the minimal model. In the context of the next-to-minimal model, we provide an estimate of the amount of doublet-singlet scalar mixing allowed by the current data.

The rest of the paper is organized as follows. In section 2 we review the consequences of various fermionic embedding for SO(5)/SO(4) as well as SO(6)/SO(5) cosets. In section 3 we present a phenomenological Lagrangian that captures the generic features of a wide class of models in terms of the Higgs coupling modifiers. Following this parametrization we perform a fit to the existing data using the χ^2 minimization technique in section 4. Finally, we draw our conclusions in section 5.

2 Composite models and modified Yukawa couplings

In this section we consider different representations for fermions in SO(5)/SO(4) and SO(6)/SO(5) cosets and work out the modifications in the top quark Yukawa coupling in a systematic manner.

2.1 SO(5)/SO(4) coset

As long as the coset is SO(5)/SO(4), the modification in VVh coupling is solely determined by ξ, as

$$k_{VVh} = \frac{g_{VVh}}{(g_{VVh})_{\rm SM}} = \sqrt{1-\xi} \simeq 1 - \frac{1}{2}\xi. \tag{2.1}$$

---

[1]$\Delta = 1/\xi$ is a measure of minimal tuning in any composite Higgs model. On top of this, an additional tuning, dubbed 'double tuning', arises in scenarios (e.g. MCHM$_{5_L-5_R}$) where the coefficients of the quadratic and quartic terms in the potential are not in the same order of the elementary-composite mixing parameter. This can be avoided when either the fermion kinetic and/or the Yukawa terms contain at least two invariants.

[2]We do not consider representation **10** of SO(5) because it does not lead to more than one Yukawa invariant keeping a discrete parity that protects the $Zb\bar{b}$ vertex [29, 51]. Note that the choice MCHM$_{14_L-1_R}$, where t_R can be fully composite, involves minimal tuning as compared to the double tuned MCHM$_{5_L-5_R}$ [30]. However, we do not consider this choice because it contains a single Yukawa invariant.

Models	$\Pi_{t_L}(q,h)$	$\Pi_{t_R}(q,h)$	$\Pi_{t_L t_R}(q,h)$
$\text{MCHM}_{5_\text{L}-5_\text{R}}$	$\Pi_0^L + \Pi_1^L \frac{h^2}{f^2}$	$\Pi_0^R + \Pi_1^R \frac{h^2}{f^2}$	$\Pi_1^{LR} \frac{h}{f} \sqrt{1 - \frac{h^2}{f^2}}$
$\text{MCHM}_{14_\text{L}-14_\text{R}}$	$\Pi_0^L + \Pi_1^L \frac{h^2}{f^2} + \Pi_2^L \frac{h^4}{f^4}$	$\Pi_0^R + \Pi_1^R \frac{h^2}{f^2} + \Pi_2^R \frac{h^4}{f^4}$	$\frac{h}{f} \sqrt{1 - \frac{h^2}{f^2}} \left(\Pi_1^{LR} + \Pi_2^{LR} \frac{h^2}{f^2} \right)$
$\text{MCHM}_{14_\text{L}-5_\text{R}}$	$\Pi_0^L + \Pi_1^L \frac{h^2}{f^2} + \Pi_2^L \frac{h^4}{f^4}$	$\Pi_0^R + \Pi_1^R \frac{h^2}{f^2}$	$\frac{h}{f} \left(\Pi_1^{LR} + \Pi_2^{LR} \frac{h^2}{f^2} \right)$
$\text{MCHM}_{5_\text{L}-14_\text{R}}$	$\Pi_0^L + \Pi_1^L \frac{h^2}{f^2}$	$\Pi_0^R + \Pi_1^R \frac{h^2}{f^2} + \Pi_2^R \frac{h^4}{f^4}$	$\frac{h}{f} \left(\Pi_1^{LR} + \Pi_2^{LR} \frac{h^2}{f^2} \right)$

Table 1. List of Π-functions, defined in eq. (2.2) for different representations.

The number of Yukawa invariants, on the other hand, depends on the representations in which t_L and t_R are embedded. We write down the relevant invariants using the pNGB representation $\Sigma = \left(0, 0, 0, h/f, \sqrt{1 - h^2/f^2} \right)^T$ in the unitary gauge:

- t_L and t_R in **5** ($\text{MCHM}_{5_\text{L}-5_\text{R}}$): $(\overline{Q}_{t_L}^5 . \Sigma)(\Sigma^T . T_{t_R}^5)$,

- t_L and t_R in **14** ($\text{MCHM}_{14_\text{L}-14_\text{R}}$): $\Sigma^T . \overline{Q}_{t_L}^{14} . T_{t_R}^{14} . \Sigma$, $(\Sigma^T . \overline{Q}_{t_L}^{14} . \Sigma)(\Sigma^T . T_{t_R}^{14} . \Sigma)$,

- t_L in **14**, t_R in **5** ($\text{MCHM}_{14_\text{L}-5_\text{R}}$): $\Sigma^T . \overline{Q}_{t_L}^{14} . T_{t_R}^5$, $(\Sigma^T . \overline{Q}_{t_L}^{14} . \Sigma)(\Sigma^T . T_{t_R}^5)$,

- t_L in **5**, t_R in **14** ($\text{MCHM}_{5_\text{L}-14_\text{R}}$): $\overline{Q}_{t_L}^5 . T_{t_R}^{14} . \Sigma$, $(\overline{Q}_{t_L}^5 . \Sigma)(\Sigma^T . T_{t_R}^{14} . \Sigma)$.

Above, Q_{t_L} and T_{t_R} contain t_L and t_R as incomplete SO(5) multiplets, respectively (see appendix A.1). The most general Lagrangian involving the top quark can be written as

$$\mathcal{L} = \bar{t}_L \slashed{q} \Pi_{t_L}(q,h) t_L + \bar{t}_R \slashed{q} \Pi_{t_R}(q,h) t_R + \bar{t}_L \Pi_{t_L t_R}(q,h) t_R + \text{h.c.} \tag{2.2}$$

The dependence on the strong sector dynamics is encoded inside the momentum dependent Π-functions. In table 1, we show the explicit forms of those functions for various representations in terms of the Higgs field with coefficients $\Pi_{0,1,2}^{L,R,LR}(q)$. The expressions for the latter in terms of the masses (m_i) and decay constants ($F_i^{L,R}$) of the strong sector resonances are given in the appendix B for the extended models, namely, $\text{MCHM}_{14_\text{L}-14_\text{R}}$, $\text{MCHM}_{14_\text{L}-5_\text{R}}$ and $\text{MCHM}_{5_\text{L}-14_\text{R}}$ respectively. The mass of the top quark and the modification of top Yukawa can be calculated from eq. (2.2) as

$$m_t = \frac{|\Pi_{t_L t_R}(q,h)|}{\sqrt{\Pi_{t_L}(q,h)\Pi_{t_R}(q,h)}} \Bigg|_{q\to 0,\ h\to v}, \quad k_{t\bar{t}h} = \frac{y_{t\bar{t}h}}{(y_{t\bar{t}h})_{\text{SM}}} = \frac{1}{(y_{t\bar{t}h})_{\text{SM}}} \left(1 - \frac{1}{2}\xi \right) \frac{\partial m_t}{\partial v}. \tag{2.3}$$

In the second equality of eq. (2.3), the factor $\left(1 - \frac{1}{2}\xi \right)$ arises due to canonical normalization of the Higgs field. As argued in [31, 67], the top quark contribution to the effective gluon-gluon-Higgs (ggh) coupling in composite Higgs models is independent of the wave function renormalization effects of the top quark due to cancellation with resonance loops. This

would imply a deviation in effective ggh coupling compared to the effective $t\bar{t}h$ coupling. The modification of the effective ggh coupling can be expressed as

$$k_{ggh}^{(t)} = \frac{c_{ggh}}{(c_{ggh})_{\mathrm{SM}}} = \frac{1}{(c_{ggh})_{\mathrm{SM}}} \left(1 - \frac{1}{2}\xi\right) \frac{\partial \log|\Pi_{t_L t_R}(q,h)|}{\partial h}\bigg|_{q\to 0,\ h\to v}. \tag{2.4}$$

The one-loop Coleman-Weinberg Higgs potential receives largest contribution from the top quark, as

$$V_{\mathrm{eff}} = -2N_c \int \frac{d^4 q}{(2\pi)^4} \log\left(q^2 \Pi_{t_L} \Pi_{t_R} + |\Pi_{t_L t_R}|^2\right) \simeq -\alpha \frac{h^2}{f^2} + \beta \frac{h^4}{f^4}. \tag{2.5}$$

The coefficients α and β above are integrals over the form factors. A similar contribution to α arises from gauge boson loops with opposite sign (largest contribution from SU(2)$_{\mathrm{L}}$ gauge bosons), parametrized as [68, 69]

$$\alpha_g \simeq -c_g \frac{1}{16\pi^2} \frac{9}{2} g^2 g_\rho^2 f^4, \tag{2.6}$$

where c_g is an $\mathcal{O}(1)$ positive constant absorbing the details of the integration, g is the SU(2)$_{\mathrm{L}}$ gauge coupling, and g_ρ corresponds to that of strong sector spin-1 resonances. The gauge contribution to β is numerically small. To calculate the top-induced contribution to α and β, we use certain parametrization of the momentum dependent form factors based on scaling arguments. The decay constants and the top-partner masses are parametrized as

$$F_i^{L,R} = \lambda_i^{L,R} f, \qquad m_i = g_i f, \tag{2.7}$$

where $\lambda_i^{L,R}$ are dimensionless constants and g_i denote strong couplings. In the present analysis, we keep $|\lambda_i|/g_i < 1$. The strong sector coupling strengths are kept well within the perturbative limits, i.e. $1 < g_i < 2\pi$. Regarding the integrals over the form factors in fermionic sector, the loop factors and the dimensionful variables are shown explicitly. Some group theoretic factors also emerge due to the decomposition of the SO(5) resonances in terms of SO(4) multiplets. We assume that sufficient number of resonances with coupling strengths g_i saturate the form factors, rendering the integrals finite. As an illustration, we show one of the integrals involved in the Higgs potential, as parametrized in [3, 68, 69]

$$\int \frac{d^4 q}{(2\pi)^4} \left(\frac{\Pi_{1,2}^{L,R}(q)}{\Pi_0^{L,R}(q)}\right)^n \simeq c_{1,2}^{(n)} \frac{1}{16\pi^2} \left(\frac{\Pi_{1,2}^{L,R}(0)}{\Pi_0^{L,R}(0)}\right)^n g_i^4 f^4, \quad n = 1, 2, \tag{2.8}$$

where $c_{1,2}^{(n)}$ are $\mathcal{O}(1)$ numbers and the forms factors are displayed in appendix B. Finally we use the following phenomenological constraints to generate the allowed parameter space:

$$\begin{aligned} 169\,\mathrm{GeV} < m_t < 176\,\mathrm{GeV}, & & v = 246\,\mathrm{GeV}, \\ 123\,\mathrm{GeV} < m_h < 127\,\mathrm{GeV}, & & 1\,\mathrm{TeV} < m_i = g_i f < 2\pi f\,. \end{aligned} \tag{2.9}$$

We present the results of our numerical analysis in figure 1. Depending on the embedding of the top quark the value of $k_{t\bar{t}h}$ varies. Interestingly, for MCHM$_{14_{\mathrm{L}}-14_{\mathrm{R}}}$ and MCHM$_{14_{\mathrm{L}}-5_{\mathrm{R}}}$
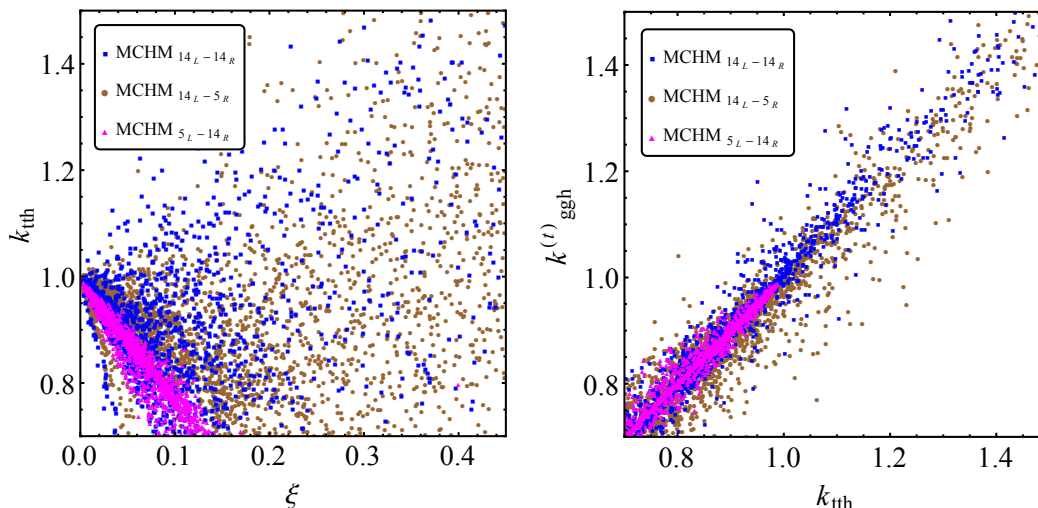
Figure 1. Results from the numerical analysis for MCHM$_{14_\text{L}-14_\text{R}}$ (blue), MCHM$_{14_\text{L}-5_\text{R}}$ (brown) and MCHM$_{5_\text{L}-14_\text{R}}$ (magenta) are shown. In the left panel $k_{t\bar{t}h}$ is plotted against ξ while at the right panel we show the correlation between $k^{(t)}_{ggh}$ and $k_{t\bar{t}h}$. While generating the model points we vary the strong couplings g_i and g_ρ in the range $[1, 2\pi]$ and $\lambda_i^{L,R}/g_i$ within $[-1, 1]$. All the points shown in the plots satisfy the phenomenological constraints given in eqs. (2.9).

we get an enhancement in top Yukawa coupling compared to its SM value ($k_{t\bar{t}h} > 1$), for a large number of model points. On the other hand, for MCHM$_{5_\text{L}-14_\text{R}}$ the top Yukawa is always suppressed. This is linked to the relative sign between the coefficients of the two Yukawa invariants. In figure 1 (right panel) we show the variation of $k^{(t)}_{ggh}$ with $k_{t\bar{t}h}$, and one observes that the two quantities are almost equal for all model points. This implies that the numerical impact of the wave function renormalization of the top quark is very small.

2.2 SO(6)/SO(5) coset

The next-to-minimal model, with SO(6)/SO(5) coset includes a real singlet scalar (η) along with the usual Higgs doublet. Quite a few interesting features emerge in this case, depending on whether η acquires a vev [21, 43, 44] or not [70–73]. In the present section we discuss the effect of the η-vev and consequently the doublet-singlet scalar mixing on the Yukawa couplings. Here we follow the convention and notation as presented in [21].

In this case the structure of the Lagrangian involving the top quark is similar to eq. (2.2), with the exception that the Π-functions are dependent both on h and η, as shown in appendix C, for different representations. Although compared to SO(5)/SO(4) coset, more possibilities of embedding t_L and t_R in different SO(6) multiplets exist, we stick to the choices shown in appendix A.2 only. The Lagrangian, in terms of the canonically normalized quantum fields (h_n, η_n), upon electroweak symmetry breaking, can be written as

$$\mathcal{L} \supset m_t \bar{t}t + k_{t\bar{t}h_n}\left(\frac{m_t}{v}\right) h_n \bar{t}t + k_{t\bar{t}\eta_n}\left(\frac{m_t}{v}\right) \eta_n \bar{t}t \,. \tag{2.10}$$

Due to the doublet-singlet mixing, the state corresponding to the observed Higgs field is

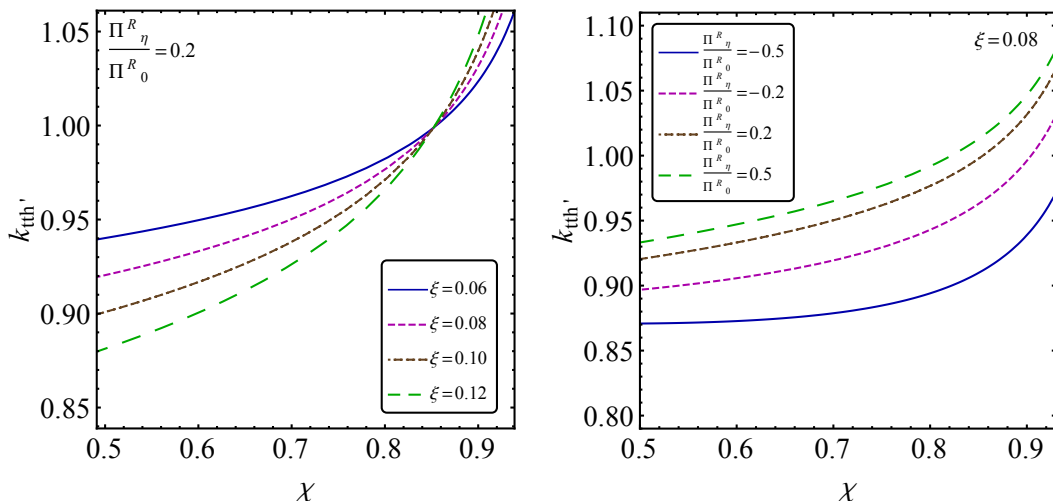$$h' = \cos\theta_\text{mix} h_n - \sin\theta_\text{mix} \eta_n \,, \tag{2.11}$$

– 6 –

Figure 2. The variation of $k_{t\bar{t}h'}$ with $\chi = \langle\eta\rangle^2/f^2$ is shown. In the left panel, for illustration, we keep the ratio Π_η^R/Π_0^R (see appendix C) fixed at 0.2, and plot the curves for different values of ξ. In the right panel we fix ξ and plot for different values of the ratio mentioned above. While plotting the curves we assume that $\Pi_1^{L,R} \ll \Pi_0^{L,R}$ and the mixing angle $\theta_{\text{mix}} < 0.25$ is respected.

where θ_{mix} denotes the amount of mixing and is constrained by the LHC Higgs data. For the case, where both $m_\eta \gg m_h$ and $\langle\eta\rangle \gg \langle h\rangle$, the mixing angle can be simply parametrized as [44]

$$\theta_{\text{mix}} \sim \frac{\langle h\rangle\langle\eta\rangle}{m_\eta^2} \ll 1\,. \tag{2.12}$$

We also observe that

$$k_{t\bar{t}\eta_n} \propto -\sqrt{\frac{\xi\chi}{1-\chi}}\,, \tag{2.13}$$

where $\chi = \langle\eta\rangle^2/f^2$. Because of an inherent $\mathcal{Z}_2$ symmetry associated with our choice of embedding, η couples with the top quark as η^2. When the $\mathcal{Z}_2$ symmetry is spontaneously broken the dependence on χ appears. The appearance of ξ is a consequence of constructing an SU(2) invariant Yukawa-like term involving the η field. Finally the expression for the Yukawa coupling modifier involving the observed Higgs is obtained as

$$k_{t\bar{t}h'} = \cos\theta_{\text{mix}}k_{t\bar{t}h_n} - \sin\theta_{\text{mix}}k_{t\bar{t}\eta_n}\,. \tag{2.14}$$

We show some representative plots illustrating the impact of χ on the Yukawa coupling modifier. In figure 2 we present the variation of $k_{t\bar{t}h'}$ with χ for NMCHM$_{6_L-6_R}$. Obviously extra model dependence appears in the case of symmetric representation (**20**), where more than one Yukawa invariant exist.

3 Effective phenomenological Lagrangian

The modifications in the Higgs couplings as discussed in the previous section have two generic features: (*i*) modification in VVh coupling, arising from the non-linearity of the

pNGBs, is universal as long as the coset belongs to $SO(N)/SO(N-1)$ group (modulo the mixing with other states), and (ii) modification of the Yukawa couplings depends on the choice of fermion embeddings. These can be captured in an effective Lagrangian as,

$$\mathcal{L} = \mathcal{L}_{\text{SMEFT}} + \Delta\mathcal{L},$$

$$\mathcal{L}_{\text{SMEFT}} \supset \partial_\mu H^\dagger \partial^\mu H + \frac{g^2}{2} H^\dagger H \left(W_\mu W^\mu + \frac{1}{2\cos\theta_w^2} Z_\mu Z^\mu \right) - \sum_u y_u \bar{q}_L H^c u_R - \sum_d y_d \bar{q}_L H d_R$$

$$- \sum_{i=u,d} \frac{\alpha_s}{8\pi} y_i b_i^s \frac{H^\dagger H}{v^2} G_{\mu\nu} G^{\mu\nu} - \frac{\alpha_{em}}{8\pi} \left(\sum_{i=u,d} y_i b_i^{em} - g b_W^{em} \right) \frac{H^\dagger H}{v^2} F_{\mu\nu} F^{\mu\nu}. \qquad (3.1)$$

Above, $\mathcal{L}_{\text{SMEFT}}$ comprises of the Standard Model effective Lagrangian with relevant dimension-4 and dimension-6 operators, where the explicit forms of the numerical coefficients b_i are given in [74]. In the $SO(5)/SO(4)$ models, additional contributions to dimension-6 operators emerge, given by

$$\Delta\mathcal{L} \supset \frac{1}{2f^2} \partial_\mu(H^\dagger H) \partial^\mu(H^\dagger H) - \sum_u (\Delta_u' + \delta_u) y_u \frac{H^\dagger H}{f^2} \bar{q}_L H^c u_R - \sum_d (\Delta_d' + \delta_d) y_d \frac{H^\dagger H}{f^2} \bar{q}_L H d_R$$

$$- \sum_{i=u,d} \frac{\alpha_s}{8\pi} \Delta_i' y_i b_i^s \frac{H^\dagger H}{f^2} G_{\mu\nu} G^{\mu\nu} - \frac{\alpha_{em}}{8\pi} \sum_{i=u,d} \Delta_i' y_i b_i^{em} \frac{H^\dagger H}{f^2} F_{\mu\nu} F^{\mu\nu}. \qquad (3.2)$$

In the above Lagrangian we have dropped terms which are highly constrained by the electroweak precision observables [45]. One can read off the Yukawa and $ggh/\gamma\gamma h$ coupling modifiers as

$$k_{f\bar{f}h} = 1 + \left(\Delta_f' + \delta_f - \frac{1}{2} \right) \xi \equiv 1 + (\Delta_f + \delta_f)\xi, \quad k_{ggh/\gamma\gamma h}^{(f)} = 1 + \left(\Delta_f' - \frac{1}{2} \right) \xi \equiv 1 + \Delta_f \xi, \tag{3.3}$$

and the modifier for VVh coupling as

$$k_{VVh} = 1 - \frac{1}{2}\xi. \tag{3.4}$$

While ξ represents the ratio of the weak scale to the effective scale of the theory, thus naturally controlling the coupling modifiers, a brief discussion of the other two parameters, namely Δ and δ, in the effective Lagrangian is in order. The origin of Δ can be traced back to the nonlinear realization of the pNGB sector. In scenarios containing only one Yukawa invariant this is a numerical constant (e.g. in MCHM$_{5_L-5_R}$, $\Delta \simeq -3/2$), while in the extended models with several invariants this factor may deviate depending on the details of the strong sector resonances. In contrast, δ reflects the effect of partial composite nature of the top quark in these theories, contributing to the anomalous dimension of the top quark. In the effective ggh and $\gamma\gamma h$ vertex, in fact, contributions from the wave function renormalization cancel against the resonance loop contributions [31, 67]. In our phenomenological analysis, that follows in the next section, we will employ the effective Lagrangian (eqs. (3.1) and (3.2)), to confront the LHC Higgs data. All fitting are done assuming Δ_t and δ_t to be free parameters. Further we assume that the bottom and τ

Modifiers	Dependence on parameters
$k_{VVh}\ (VV = WW, ZZ)$	$1 - \frac{1}{2}\xi$
$k_{t\bar{t}h}$	$1 + (\Delta_t + \delta_t)\,\xi$
$k_{ggh/\gamma\gamma h}^{(t)}$	$1 + \Delta_t\xi$
$k_{b\bar{b}h}$	$1 - \frac{3}{2}\xi$
$k_{ggh}^{(b)}$	$1 - \frac{3}{2}\xi$
$k_{\tau\bar{\tau}h}$	$1 - \frac{3}{2}\xi$

Table 2. Scaling of the Higgs effective couplings for SO(5)/SO(4) model.

Yukawa couplings are modified only by the universal factor $\Delta_b = \Delta_\tau = -3/2$, i.e. they are always suppressed compared to their SM values. We also make a reasonable approximation $\delta_b = \delta_\tau = 0$. A complete list of all the coupling modifiers within the SO(5)/SO(4) model is given in table 2.[3] The explicit expressions of Δ_t and δ_t in terms of the form factors are defined in table 5 of appendix D.

The main feature that gets added when one moves to the next-to-minimal model is the presence of an additional singlet scalar and its mixing with the Higgs doublet. A description of the composite models including a SM singlet in the context of a strongly interacting light Higgs can be found in [75]. Here we present a simplified effective Lagrangian keeping only the dominant terms. We add the following piece involving η to eqs. (3.1) and (3.2),

$$\Delta\mathcal{L}_\eta \sim \frac{1}{2}\partial_\mu\eta\partial^\mu\eta - \sum_u y_u(\Delta_u^\eta)'\frac{\eta^2}{f^2}\bar{q}_L H^c u_R - \sum_d y_d(\Delta_d^\eta)'\frac{\eta^2}{f^2}\bar{q}_L H d_R\,. \tag{3.5}$$

Note that the dimension-5 operators involving a single η field is not allowed in the presence of a $\mathcal{Z}_2$ symmetry, as discussed in previous section. Due to doublet-singlet scalar mixing (θ_{mix}), the Yukawa modifier for the observed Higgs boson (h') assumes the following form

$$k_{f\bar{f}h'} = \cos\theta_{\mathrm{mix}}\,(1 + (\Delta_f + \delta_f)\xi) + \sin\theta_{\mathrm{mix}}\Delta_f^\eta\sqrt{\xi}\,, \tag{3.6}$$

where Δ_f^η is a function of $(\Delta_f^\eta)'$ and the η-vev. The expressions for Δ_t^η for different representations are given in table 6 of appendix D. In the following analysis we assume $\Delta_t^\eta = \Delta_b^\eta$ for simplicity.

The VVh' coupling modifier now picks up the additional factor $\cos\theta_{\mathrm{mix}}$ compared to the minimal coset (see eq. (3.4))

$$k_{VVh'} = \cos\theta_{\mathrm{mix}}\sqrt{1 - \xi}\,. \tag{3.7}$$

---

[3]In [53], effective ggh and $\gamma\gamma h$ coupling modifiers have been calculated keeping only the dominant terms: $k_{ggh} \simeq 1.06\,(k_{ggh}^{(t)})^2 + 0.01\,(k_{ggh}^{(b)})^2 - 0.07\,k_{ggh}^{(b)}k_{ggh}^{(t)}$ and $k_{\gamma\gamma h} \simeq 0.07\,(k_{\gamma\gamma h}^{(t)})^2 + 1.59\,k_{WWh}^2 - 0.66\,k_{\gamma\gamma h}^{(t)}k_{WWh}$.

4 Constraints from LHC Run 1 and Run 2 Higgs data

In this section we discuss how the Higgs coupling modifications confront the recent LHC data [53–66]. We perform a χ^2 fit to assess the present constraints starting from the effective Lagrangian introduced in the previous section. We use the combined ATLAS+CMS Run 1 results for signal strengths, given by the 'six-parameter' fit as shown in table 15 of [53]. The so far available Run 2 (13 TeV) results are summarized in table 3.

The effective Lagrangian given in eq. (3.2), which corresponds to SO(5)/SO(4) coset, have three independent parameters ξ, Δ_t and δ_t. Using this parametrization we calculate the Higgs signal strengths in various final states normalized to their SM values. These are then compared with the data using the χ^2 fit. The minimum value of the χ^2 and corresponding best-fit values of the parameters in the extended models are given below.

- Run 1:
$$\chi^2_{\min} = 1.92, \quad \Delta_t = -0.31, \quad \delta_t = 0.10, \quad \xi = 0.13, \tag{4.1}$$

- Run 1 + Run 2:
$$\chi^2_{\min} = 18.85, \quad \Delta_t = -0.06, \quad \delta_t = 0.02, \quad \xi = 0.05. \tag{4.2}$$

This may be compared with a similar fit obtained for the MCHM$_{5_{\rm L}-5_{\rm R}}$ with only one free parameter ξ. The best-fit values are given by

- Run 1:
$$\chi^2_{\min} = 3.43, \quad \xi = 0.007, \tag{4.3}$$

- Run 1 + Run 2:
$$\chi^2_{\min} = 19.72, \quad \xi = 0.00. \tag{4.4}$$

In figures 3 we plot $\Delta\chi^2$ as a function of ξ, corresponding to our effective Lagrangian eq. (3.2), with all other parameters fixed to their best-fit values. For comparison, we also show the curve for MCHM$_{5_{\rm L}-5_{\rm R}}$, and our results agree with [44] wherever we overlap. For the extended models, we obtain a lower bound $f \geq 465$ GeV at 95% CL from Run 1 data only. This should be compared with $f \geq 780$ GeV at 95% CL for MCHM$_{5_{\rm L}-5_{\rm R}}$. The relaxation of the bounds on f for the extended models follows from the reduced correlation between $k_{t\bar{t}h}$ and k_{VVh} in the effective Lagrangian in eq. (3.2) as compared to the tight correlation in MCHM$_{5_{\rm L}-5_{\rm R}}$. We find that combined Run 1 and Run 2 data give significantly more stringent lower bound, namely, $f \geq 640$ GeV at 95% CL for the extended models.

In figures 4 we check whether the extended models fit the data better (i.e. $\chi^2/d.o.f.$ is lower) than MCHM$_{5_{\rm L}-5_{\rm R}}$. In the blue shaded region the extended models, as parametrically encoded in the effective Lagrangian in eq. (3.2), fit relatively better for the entire range of ξ. On the same plot we also throw the actual model points, with the resonance masses and decay constants as the strong sector inputs, discussed on a case-by-case basis in section 2.1, satisfying the constraints shown in eq. (2.9). In figures 5, the experimentally preferred regions for the coupling modifiers are shown at 68% and 95% CL in the ($k_{t\bar{t}h}$–ξ) and

Run 2 Data				
Collaboration	References	Decay Channels	Production Modes	Results
ATLAS	[54]	WW	VBF	$1.70^{+1.10}_{-0.90}$
	[55, 56]	$\gamma\gamma$	ggF	$0.80^{+0.19}_{-0.18}$
			VBF	$2.10^{+0.60}_{-0.60}$
			VH	$0.70^{+0.90}_{-0.80}$
			$t\bar{t}H$	$0.60^{+0.70}_{-0.60}$
	[57]	ZZ^*	ggF	$1.11^{+0.25}_{-0.22}$
			VBF	$4.00^{+1.77}_{-1.46}$
	[56, 58]	$b\bar{b}$	VH	$1.20^{+0.42}_{-0.36}$
			$t\bar{t}H$	$0.80^{+0.60}_{-0.60}$
	[56, 59]	Multileptons	$t\bar{t}H$	$1.60^{+0.50}_{-0.40}$
CMS	[60]	WW	$ggF + VBF + VH$	$1.050^{+0.26}_{-0.26}$
	[61]	$\gamma\gamma$	ggF	$1.11^{+0.19}_{-0.18}$
			VBF	$0.50^{+0.60}_{-0.50}$
			VH	$2.30^{+1.10}_{-1.00}$
			$t\bar{t}H$	$2.20^{+0.90}_{-0.80}$
	[62]	ZZ^*	$ggF + t\bar{t}H$	$1.20^{+0.35}_{-0.31}$
	[63]	$\tau\tau$	$ggF + VBF + VH$	$1.06^{+0.25}_{-0.24}$
	[64]	$b\bar{b}$	ZH	$1.20^{+0.40}_{-0.40}$
	[65]	τ_h+others	$t\bar{t}H$	$0.72^{+0.62}_{-0.53}$
	[66]	Multileptons	$t\bar{t}H$	$1.50^{+0.50}_{-0.50}$

Table 3. Results from the ATLAS and CMS collaborations for Higgs signal strengths at 13 TeV are tabulated.

$(k^{(t)}_{ggh} - k_{t\bar{t}h})$ planes. The model points are observed to span over a large range of the preferred regions. It may be noted that present experimental precision is not sensitive to the value of δ_t separately; what is in fact bounded is the combination $(\Delta_t + \delta_t)$. Future colliders may have sufficient precision to sense the different modifications in the top Yukawa coupling and the effective ggh coupling.

Moving to the next-to-minimal coset, we deal with a new feature that the Higgs doublet now mixes with a real singlet. The mixing results in a further suppression of the observed Higgs boson coupling to the massive gauge bosons. The Yukawa couplings are modified too because of the presence of a singlet. We perform a similar χ^2 analysis with the combined Run 1 and Run 2 results to impose an upper bound on the amount of mixing. Figure 6 shows that the maximum amount of mixing allowed so far at 95% CL is $\theta_{\mathrm{mix}} \sim 0.35$. Future data would constrain it even further [21].
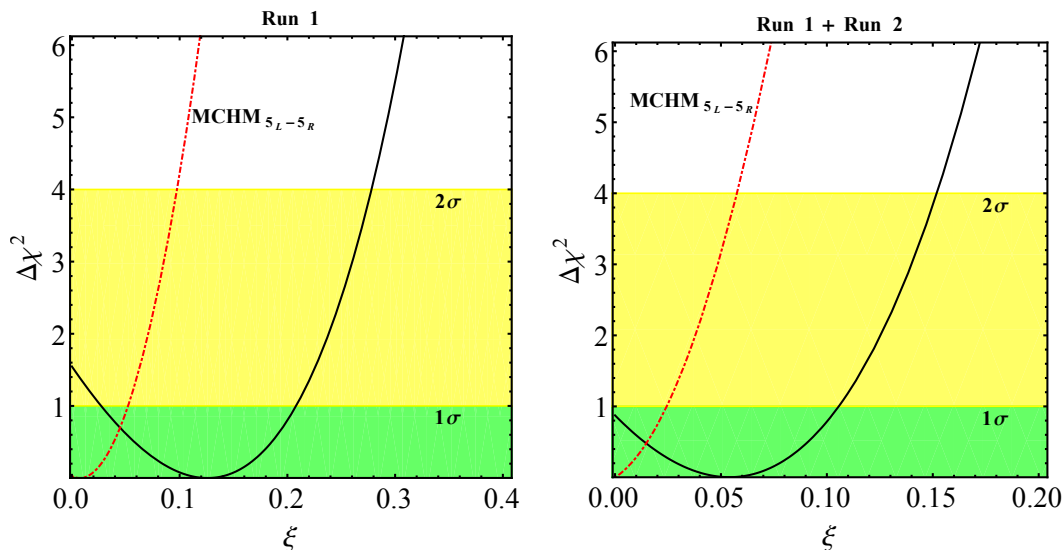
Figure 3. Results of χ^2 analysis for Run 1 and Run 1 + Run 2 datasets are shown in the left and right panels, respectively. Solid black line represents $\Delta\chi^2 = \chi^2 - \chi^2_{\min}$ for the extended models, while the red dashed lines represents the same for MCHM$_{5_L-5_R}$. Green and yellow regions denote the allowed range for ξ at 68% and 95% CL, respectively.
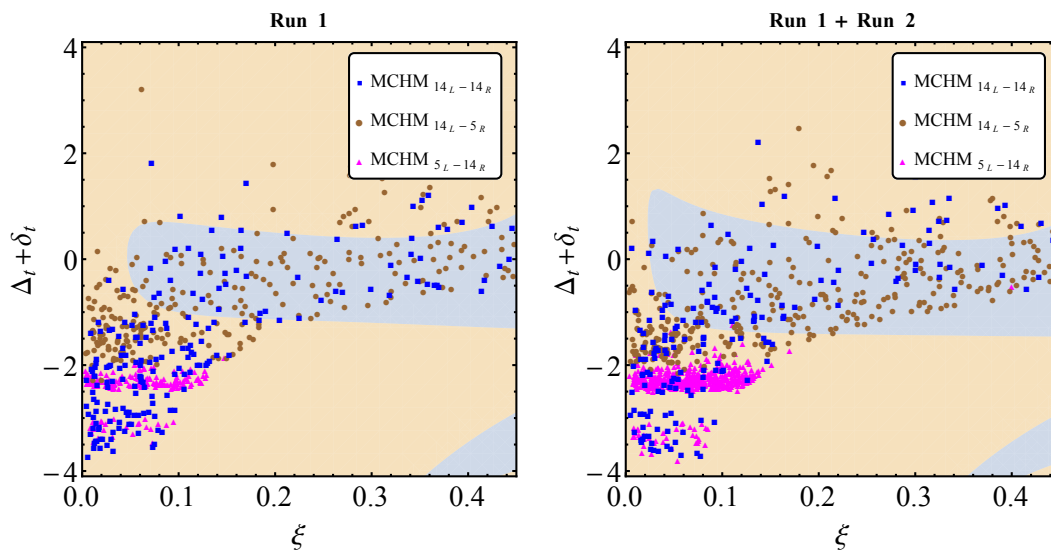

Figure 4. In both the left and right panels, blue shaded regions denote relatively lower values of $\chi^2/d.o.f.$ for the extended models, given by the effective Lagrangian in eq. (3.2), compared to the MCHM$_{5_L-5_R}$. Model points, with resonance masses and decay constants as inputs, satisfying the constraints of eq. (2.9), are superimposed.

5   Conclusions

Non-linearity of pNGB dynamics modifies the Higgs boson couplings with the weak gauge bosons as well as with the fermions compared to their SM expectations. The ratio ξ, which parametrizes the hierarchy between the weak scale and the strong sector spontaneous
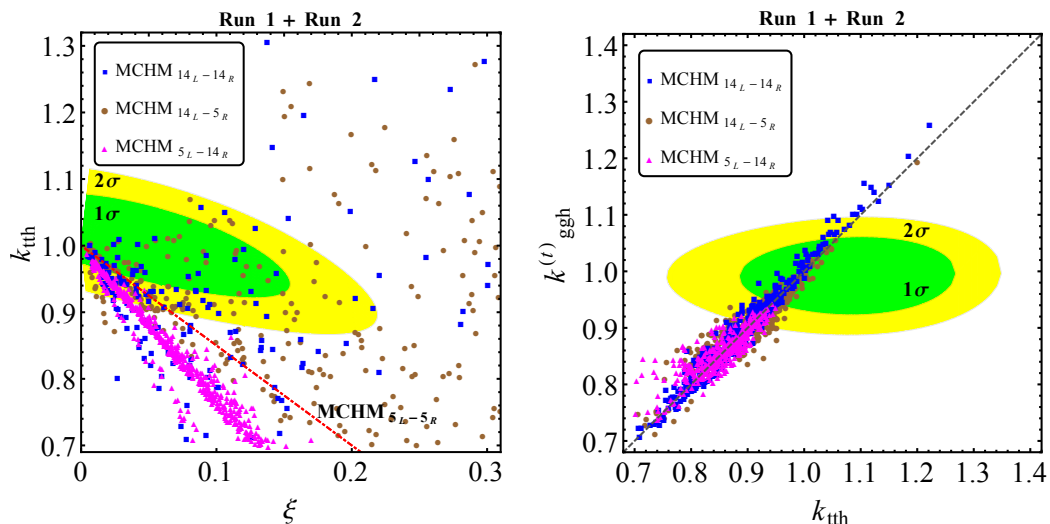
Figure 5. We present the regions in the $k_{t\bar{t}h} - \xi$ and $k_{ggh}^{(t)} - k_{t\bar{t}h}$ planes allowed at 68% (green) and 95% (yellow) CL using combined Run 1 and available Run 2 data. In the left panel the red line corresponds to MCHM$_{5_L-5_R}$. On the right panel, the grey dashed line corresponds to $\delta_t = 0$. Valid 'extended model' points are observed to lie within the experimentally allowed regions.
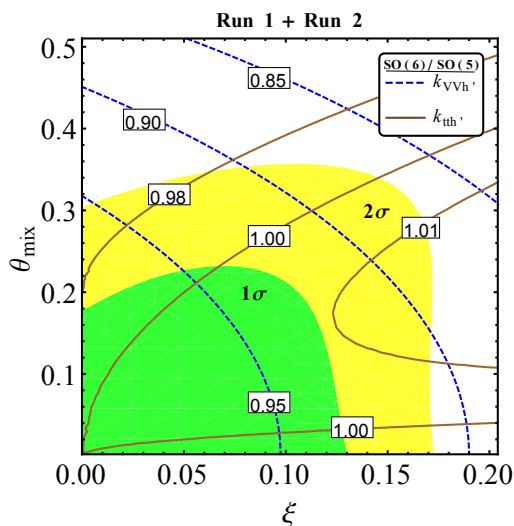

Figure 6. For the next-to-minimal model, the allowed regions in the $\theta_{\rm mix} - \xi$ plane at 68% (green) and 95% (yellow) CL are shown using the combined Run 1 and available Run 2 data. The brown lines represent the contours of fixed $k_{t\bar{t}h'}$, while the blue dashed lines correspond to that of $k_{VVh'}$.

symmetry breaking scale, controls this deformation. In MCHM$_{5_L-5_R}$, the Yukawa sector contains a single invariant. Here, the single parameter ξ appears in the modifications of both VVh and $f\bar{f}h$ couplings, leading to a rather strong lower limit $f \geq 1\,{\rm TeV}$, as the data show increasing affinity towards the SM predictions. In the extended models, MCHM$_{14_L-14_R}$, MCHM$_{14_L-5_R}$ and MCHM$_{5_L-14_R}$, owing to the presence of more than one invariant in the Yukawa sector, the $f\bar{f}h$ coupling modifier depends on other parameters of

the strong sector in addition to ξ. This releases the tension leading to a new lower limit $f \geq 640\,\mathrm{GeV}$, which is much relaxed compared to the limit in $\mathrm{MCHM}_{5_\mathrm{L}-5_\mathrm{R}}$.

An important feature of these models is the emergence of a parametric difference in the top Yukawa and the effective gluon-gluon-Higgs vertices. This arises because of a cancellation between the top-partner resonance masses in the loop with the wave function renormalization of the top quark in the calculation of the effective ggh vertex. However, the present data is insensitive to smell this difference.

We have in fact constructed a phenomenological Lagrangian which captures the effects of a vast array of such models with different fermionic representations. We have constrained the parameters of this Lagrangian using LHC data and observed that the allowed regions are quite consistent with a reasonable choice of strong sector input parameters of the individual models which yield correct values of m_t, v and m_h.

We have extended our analysis to the next-to-minimal model as well. The appearance of a real singlet scalar adds a new twist to phenomenology, whose mixing with the Higgs doublet is constrained by the LHC data. Interestingly, the singlet scalar also contributes to the top Yukawa through an effective higher dimensional operator.

Our analysis shows that further precision, likely to be achieved in future colliders, would constrain these scenarios to the extent that individual models could be discriminated, and the proposition that the Higgs boson may have a spatial extension would be challenged with more ammunition.

Acknowledgments

A Fermion embeddings

A.1 SO(5)/SO(4) coset

Fundamental $\mathbf{5}$ and symmetric $\mathbf{14}$ representations of SO(5) can be decomposed under the unbroken $\mathrm{SO}(4) \equiv \mathrm{SU}(2)_\mathrm{L} \times \mathrm{SU}(2)_\mathrm{R}$ as follows:

$$
\begin{aligned}
\mathbf{5} &= \mathbf{1} \oplus \mathbf{4} = (\mathbf{1},\mathbf{1}) \oplus (\mathbf{2},\mathbf{2}), \\
\mathbf{14} &= \mathbf{1} \oplus \mathbf{4} \oplus \mathbf{9} = (\mathbf{1},\mathbf{1}) \oplus (\mathbf{2},\mathbf{2}) \oplus (\mathbf{3},\mathbf{3}).
\end{aligned}
\tag{A.1}
$$

We embed t_L into the $(\mathbf{2},\mathbf{2})$'s so that the correction to $Zb\bar{b}$ vertex is under control, while t_R is embedded into the $(\mathbf{1},\mathbf{1})$. The embeddings of the top quarks into incomplete multiplets of $\mathbf{5}$ and $\mathbf{14}$ are given below.

$$Q^5_{t_L} = \left(\Psi_{(2,2)}, 0 \right)^T, \quad T^5_{t_R} = (0,0,0,0,t_R)^T, \tag{A.2}$$

and

$$Q^{14}_{t_L} = \left(\begin{array}{c|c} 0_{4\times 4} & \frac{\Psi^T_{(2,2)}}{\sqrt{2}} \\ \hline \frac{\Psi_{(2,2)}}{\sqrt{2}} & 0 \end{array} \right), \quad T^{14}_{t_R} = \left(\begin{array}{c|c} -\frac{t_R}{2\sqrt{5}}I_4 & 0_{4\times 1} \\ \hline 0_{1\times 4} & 4\frac{t_R}{2\sqrt{5}} \end{array} \right), \tag{A.3}$$

where

$$\Psi_{(2,2)} = \frac{1}{\sqrt{2}}(ib_L, b_L, it_L, -t_L). \tag{A.4}$$

A.2 SO(6)/SO(5) coset

Decomposition of different representations of SO(6), used in the main text, under the maximal subgroup $\text{SO}(6) \supset \text{SO}(4) \times \text{SO}(2) \simeq \text{SU}(2)_L \times \text{SU}(2)_R \times \text{U}(1)_\eta$, is as follows:

$$\begin{aligned}
\mathbf{6}_0 &= (\mathbf{2},\mathbf{2})_0 \oplus (\mathbf{1},\mathbf{1})_2 \oplus (\mathbf{1},\mathbf{1})_{-2}, \\
\mathbf{15}_0 &= (\mathbf{1},\mathbf{1})_0 \oplus (\mathbf{2},\mathbf{2})_2 \oplus (\mathbf{2},\mathbf{2})_{-2} \oplus (\mathbf{3},\mathbf{1})_0 \oplus (\mathbf{1},\mathbf{3})_0, \\
\mathbf{20}_0 &= (\mathbf{1},\mathbf{1})_0 \oplus (\mathbf{1},\mathbf{1})_4 \oplus (\mathbf{1},\mathbf{1})_{-4} \oplus (\mathbf{2},\mathbf{2})_2 \oplus (\mathbf{2},\mathbf{2})_{-2} \oplus (\mathbf{3},\mathbf{3})_0,
\end{aligned} \tag{A.5}$$

where the subscripts denote the charges under $\text{U}(1)_\eta$. Embedding of t_L and t_R in the above representations are given as

$$Q^6_{t_L} = \left(\Psi_{(2,2)}, 0, 0 \right)^T, \qquad T^6_{t_R} = (0,0,0,0,0,t_R)^T, \tag{A.6}$$

$$Q^{15}_{t_L} = \left(\begin{array}{c|c} 0_{4\times 4} & 0 \ \frac{\Psi^T_{(2,2)}}{\sqrt{2}} \\ \hline 0 & \\ -\frac{\Psi_{(2,2)}}{\sqrt{2}} & 0_{2\times 2} \end{array} \right), \quad T^{15}_{t_R} = \left(\begin{array}{cc|c} \begin{array}{cc} 0 & -i\frac{t_R}{2} \\ i\frac{t_R}{2} & 0 \end{array} & 0_{2\times 2} & \\ \hline 0_{2\times 2} & \begin{array}{cc} 0 & i\frac{t_R}{2} \\ -i\frac{t_R}{2} & 0 \end{array} & 0_{4\times 2} \\ \hline 0_{2\times 4} & & 0_{2\times 2} \end{array} \right), \tag{A.7}$$

and

$$Q^{20}_{t_L} = \left(\begin{array}{c|c} 0_{4\times 4} & 0 \ \frac{\Psi^T_{(2,2)}}{\sqrt{2}} \\ \hline 0 & \\ \frac{\Psi_{(2,2)}}{\sqrt{2}} & 0_{2\times 2} \end{array} \right), \quad T^{20}_{t_R} = \left(\begin{array}{c|c} -\frac{t_R}{2\sqrt{3}}I_4 & 0_{4\times 2} \\ \hline 0_{2\times 4} & \frac{t_R}{\sqrt{3}}I_2 \end{array} \right). \tag{A.8}$$

B Details of form factors

The form factors appearing in table 1 can be decomposed under unbroken SO(4) and written in terms of masses and decay constants of the resonances. Detailed expressions of the form factors for $\text{MCHM}_{14_L-14_R}$, $\text{MCHM}_{14_L-5_R}$ and $\text{MCHM}_{5_L-14_R}$ models are listed below (for explicit calculations see [31]).

MCHM$_{14_L-14_R}$

$$\Pi_0^L = 1 + \frac{|F_4^L|^2}{q^2 + m_4^2},$$

$$\Pi_1^L = \left(\frac{5}{4} \frac{|F_1^L|^2}{q^2 + m_1^2} - \frac{5}{2} \frac{|F_4^L|^2}{q^2 + m_4^2} + \frac{5}{4} \frac{|F_9^L|^2}{q^2 + m_9^2} \right),$$

$$\Pi_2^L = \left(-\frac{5}{4} \frac{|F_1^L|^2}{q^2 + m_1^2} + 2\frac{|F_4^L|^2}{q^2 + m_4^2} - \frac{3}{4} \frac{|F_9^L|^2}{q^2 + m_9^2} \right),$$

$$\Pi_0^R = 1 + \frac{|F_1^R|^2}{q^2 + m_1^2},$$

$$\Pi_1^R = \left(\frac{5}{2} \frac{|F_4^R|^2}{q^2 + m_4^2} - \frac{5}{2} \frac{|F_1^R|^2}{q^2 + m_1^2} \right),$$

$$\Pi_2^R = \left(\frac{25}{16} \frac{|F_1^R|^2}{q^2 + m_1^2} - \frac{5}{2} \frac{|F_4^R|^2}{q^2 + m_4^2} + \frac{15}{16} \frac{|F_9^R|^2}{q^2 + m_9^2} \right),$$

$$\Pi_1^{LR} = -\frac{\sqrt{5}}{2} \left(\frac{F_1^L F_1^{R*} m_1}{q^2 + m_1^2} - \frac{F_4^L F_4^{R*} m_4}{q^2 + m_4^2} \right),$$

$$\Pi_2^{LR} = -\left(-\frac{5\sqrt{5}}{8} \frac{F_1^L F_1^{R*} m_1}{q^2 + m_1^2} + \sqrt{5}\frac{F_4^L F_4^{R*} m_4}{q^2 + m_4^2} - \frac{3\sqrt{5}}{8} \frac{F_9^L F_9^{R*} m_9}{q^2 + m_9^2} \right).$$

(B.1)

MCHM$_{14_L-5_R}$

$$\Pi_0^L = 1 + \frac{|F_4^L|^2}{q^2 + m_4^2},$$

$$\Pi_1^L = \frac{5}{4} \frac{|F_1^L|^2}{q^2 + m_1^2} - \frac{5}{2} \frac{|F_4^L|^2}{q^2 + m_4^2} + \frac{5}{4} \frac{|F_9^L|^2}{q^2 + m_4^2},$$

$$\Pi_2^L = 2\frac{|F_4^L|^2}{q^2 + m_4^2} - \frac{5}{4} \frac{|F_1^L|^2}{q^2 + m_1^2} - \frac{3}{4} \frac{|F_9^L|^2}{q^2 + m_4^2},$$

$$\Pi_0^R = 1 + \frac{|F_1^R|^2}{q^2 + m_1^2},$$

$$\Pi_1^R = \frac{|F_4^R|^2}{q^2 + m_4^2} - \frac{|F_1^R|^2}{q^2 + m_1^2},$$

$$\Pi_1^{LR} = \frac{1}{\sqrt{2}} \frac{F_4^L F_4^{R*} m_4}{q^2 + m_4^2} - \frac{\sqrt{5}}{2} \frac{F_1^L F_1^{R*} m_1}{q^2 + m_1^2},$$

$$\Pi_2^{LR} = \frac{\sqrt{5}}{2} \frac{F_1^L F_1^{R*} m_1}{q^2 + m_1^2} - \sqrt{2}\frac{F_4^L F_4^{R*} m_4}{q^2 + m_4^2}.$$

(B.2)

MCHM$_{5_L-14_R}$

$$\Pi_0^L = 1 + \frac{|F_4^L|^2}{q^2 + m_4^2}$$

$$\Pi_1^L = \frac{1}{2} \left(\frac{|F_1^L|^2}{q^2 + m_1^2} - \frac{|F_4^L|^2}{q^2 + m_4^2} \right)$$

$$\Pi_0^R = 1 + \frac{|F_1^R|^2}{q^2 + m_1^2}$$

$$\Pi_1^R = \frac{5}{2} \left(\frac{|F_4^R|^2}{q^2 + m_4^2} - \frac{|F_1^R|^2}{q^2 + m_1^2} \right)$$

$$\Pi_2^R = \frac{25}{16} \frac{|F_1^R|^2}{q^2 + m_1^2} - \frac{5}{2} \frac{|F_4^R|^2}{q^2 + m_4^2} + \frac{15}{16} \frac{|F_9^R|^2}{q^2 + m_4^2}$$

$$\Pi_1^{LR} = \frac{\sqrt{5}}{2} \frac{F_4^L F_4^{R*} m_4}{q^2 + m_4^2} - \frac{1}{\sqrt{2}} \frac{F_1^L F_1^{R*} m_1}{q^2 + m_1^2}$$

$$\Pi_2^{LR} = \frac{5\sqrt{2}}{8} \frac{F_1^L F_1^{R*} m_1}{q^2 + m_1^2} - \frac{\sqrt{5}}{2} \frac{F_4^L F_4^{R*} m_4}{q^2 + m_4^2}$$

(B.3)

C Π-functions for next-to-minimal models

The Π-functions for the next-to-minimal case are given for different representations in table 4. The NMCHM$_{15_L-1_R}$ case is not included in the table because it cannot generate a Yukawa term in the Lagrangian.

Models	$\Pi_{t_L}(h,\eta)$	$\Pi_{t_R}(h,\eta)$	$\Pi_{t_L t_R}(h,\eta)$
NMCHM$_{6_L-1_R}$	$\Pi_0^L + \Pi_1^L \frac{h^2}{f^2}$	Π_0^R	$\Pi_1^{LR}\frac{h}{f}$
NMCHM$_{6_L-6_R}$	$\Pi_0^L + \Pi_1^L \frac{h^2}{f^2}$	$\Pi_0^R + \Pi_1^R \frac{h^2}{f^2} + \Pi_\eta^R \frac{\eta^2}{f^2}$	$\Pi_1^{LR}\frac{h}{f}\sqrt{1 - \frac{h^2}{f^2} - \frac{\eta^2}{f^2}}$
NMCHM$_{6_L-15_R}$	$\Pi_0^L + \Pi_1^L \frac{h^2}{f^2}$	$\Pi_0^R + \Pi_1^R \frac{h^2}{f^2}$	$\Pi_1^{LR}\frac{h}{f}$
NMCHM$_{6_L-20_R}$	$\Pi_0^L + \Pi_1^L \frac{h^2}{f^2}$	$\Pi_0^R + \Pi_1^R \frac{h^2}{f^2} + \Pi_2^R \frac{h^4}{f^4}$	$\frac{h}{f}\left(\Pi_1^{LR} + \Pi_2^{LR}\frac{h^2}{f^2}\right)$
NMCHM$_{15_L-6_R}$	$\Pi_0^L + \Pi_1^L \frac{h^2}{f^2} + \Pi_\eta^L \frac{\eta^2}{f^2}$	$\Pi_0^R + \Pi_1^R \frac{h^2}{f^2} + \Pi_\eta^R \frac{\eta^2}{f^2}$	$\Pi_1^{LR}\frac{h}{f}$
NMCHM$_{15_L-15_R}$	$\Pi_0^L + \Pi_1^L \frac{h^2}{f^2} + \Pi_\eta^L \frac{\eta^2}{f^2}$	$\Pi_0^R + \Pi_1^R \frac{h^2}{f^2}$	$\Pi_1^{LR}\frac{h}{f}\sqrt{1 - \frac{h^2}{f^2} - \frac{\eta^2}{f^2}}$
NMCHM$_{15_L-20_R}$	$\Pi_0^L + \Pi_1^L \frac{h^2}{f^2} + \Pi_\eta^L \frac{\eta^2}{f^2}$	$\Pi_0^R + \Pi_1^R \frac{h^2}{f^2} + \Pi_2^R \frac{h^4}{f^4}$	$\Pi_1^{LR}\frac{h}{f}\sqrt{1 - \frac{h^2}{f^2} - \frac{\eta^2}{f^2}}$
NMCHM$_{20_L-1_R}$	$\Pi_0^L + \Pi_1^L \frac{h^2}{f^2} + \Pi_2^L \frac{h^4}{f^4}$ $+\Pi_\eta^L \frac{\eta^2}{f^2} + \Pi_{h\eta}^L \frac{h^2}{f^2}\frac{\eta^2}{f^2}$	Π_0^R	$\Pi_1^{LR}\frac{h}{f}\sqrt{1 - \frac{h^2}{f^2} - \frac{\eta^2}{f^2}}$
NMCHM$_{20_L-6_R}$	$\Pi_0^L + \Pi_1^L \frac{h^2}{f^2} + \Pi_2^L \frac{h^4}{f^4}$ $+\Pi_\eta^L \frac{\eta^2}{f^2} + \Pi_{h\eta}^L \frac{h^2}{f^2}\frac{\eta^2}{f^2}$	$\Pi_0^R + \Pi_1^R \frac{h^2}{f^2} + \Pi_\eta^R \frac{\eta^2}{f^2}$	$\frac{h}{f}\left(\Pi_1^{LR} + \Pi_2^{LR}\frac{h^2}{f^2} + \Pi_\eta^{LR}\frac{\eta^2}{f^2}\right)$
NMCHM$_{20_L-15_R}$	$\Pi_0^L + \Pi_1^L \frac{h^2}{f^2} + \Pi_2^L \frac{h^4}{f^4}$ $+\Pi_\eta^L \frac{\eta^2}{f^2} + \Pi_{h\eta}^L \frac{h^2}{f^2}\frac{\eta^2}{f^2}$	$\Pi_0^R + \Pi_1^R \frac{h^2}{f^2}$	$\Pi_1^{LR}\frac{h}{f}\sqrt{1 - \frac{h^2}{f^2} - \frac{\eta^2}{f^2}}$
NMCHM$_{20_L-20_R}$	$\Pi_0^L + \Pi_1^L \frac{h^2}{f^2} + \Pi_2^L \frac{h^4}{f^4}$ $+\Pi_\eta^L \frac{\eta^2}{f^2} + \Pi_{h\eta}^L \frac{h^2}{f^2}\frac{\eta^2}{f^2}$	$\Pi_0^R + \Pi_1^R \frac{h^2}{f^2} + \Pi_2^R \frac{h^4}{f^4}$	$\frac{h}{f}\sqrt{1 - \frac{h^2}{f^2} - \frac{\eta^2}{f^2}}\left(\Pi_1^{LR} + \Pi_2^{LR}\frac{h^2}{f^2}\right)$

Table 4. List of Π-functions for different representations of next-to-minimal model.

D Expressions for Δ_t, δ_t and Δ_t^η

In table 5 we list the expressions for Δ_t and δ_t for the models MCHM$_{5_L-5_R}$, MCHM$_{14_L-14_R}$, MCHM$_{14_L-5_R}$ and MCHM$_{5_L-14_R}$, respectively.

Models	Δ_t	δ_t
MCHM$_{5_L-5_R}$	$-\frac{3}{2}$	$-\left(\frac{\Pi_1^L}{\Pi_0^L} + \frac{\Pi_1^R}{\Pi_0^R}\right)$
MCHM$_{14_L-14_R}$	$2\frac{\Pi_2^{LR}}{\Pi_1^{LR}} - \frac{3}{2}$	$-\left(\frac{\Pi_1^L}{\Pi_0^L} + \frac{\Pi_1^R}{\Pi_0^R}\right)$
MCHM$_{14_L-5_R}$	$2\frac{\Pi_2^{LR}}{\Pi_1^{LR}} - \frac{1}{2}$	$-\left(\frac{\Pi_1^L}{\Pi_0^L} + \frac{\Pi_1^R}{\Pi_0^R}\right)$
MCHM$_{5_L-14_R}$	$2\frac{\Pi_2^{LR}}{\Pi_1^{LR}} - \frac{1}{2}$	$-\left(\frac{\Pi_1^L}{\Pi_0^L} + \frac{\Pi_1^R}{\Pi_0^R}\right)$

Table 5. Expressions for Δ_t and δ_t for different representations of SO(5) in which top quark is embedded.

We present the expressions for $(\Delta_t + \delta_t)$ and Δ_t^η, as defined in eq. (2.12), in terms of the form factors, for different SO(6) representations in table 6.

Models		Coupling Modifiers
NMCHM$_{6_L-1_R}$	$\Delta_t + \delta_t$	$-\left(\frac{\Pi_1^L}{\Pi_0^L} + \frac{1}{2}\right)$
	Δ_t^η	0
NMCHM$_{6_L-6_R}$	$\Delta_t + \delta_t$	$-\left(1 + \frac{\Pi_\eta^R}{\Pi_0^R}\chi\right)^{-1}\left[\frac{\Pi_1^L}{\Pi_0^L} + \frac{\Pi_1^R}{\Pi_0^R} + \frac{3}{2} + \left(\frac{\Pi_1^L}{\Pi_0^L}\frac{\Pi_\eta^R}{\Pi_0^R} + \frac{1}{2}\frac{\Pi_\eta^R}{\Pi_0^R}\right)\chi\right]$
	Δ_t^η	$\left(1 + \frac{\Pi_\eta^R}{\Pi_0^R}\right)\left(1 + \frac{\Pi_\eta^R}{\Pi_0^R}\chi\right)^{-1}\sqrt{\frac{\chi}{1-\chi}}$
NMCHM$_{6_L-15_R}$	$\Delta_t + \delta_t$	$-\left[\frac{\Pi_1^L}{\Pi_0^L} + \frac{\Pi_1^R}{\Pi_0^R} + \frac{1}{2}\right]$
	Δ_t^η	0
NMCHM$_{6_L-20_R}$	$\Delta_t + \delta_t$	$\left[2\frac{\Pi_2^{LR}}{\Pi_1^{LR}} - \frac{\Pi_1^L}{\Pi_0^L} - \frac{\Pi_1^R}{\Pi_0^R} - \frac{1}{2}\right]$
	Δ_t^η	0
NMCHM$_{15_L-6_R}$	$\Delta_t + \delta_t$	$-\left(1 + \frac{\Pi_\eta^L}{\Pi_0^L}\chi\right)^{-1}\left(1 + \frac{\Pi_\eta^R}{\Pi_0^R}\chi\right)^{-1}\left[\frac{\Pi_1^L}{\Pi_0^L} + \frac{\Pi_1^R}{\Pi_0^R} + \frac{1}{2} - \left(\frac{1}{2}\frac{\Pi_\eta^L}{\Pi_0^L} + \frac{1}{2}\frac{\Pi_\eta^R}{\Pi_0^R} - \frac{\Pi_1^L}{\Pi_0^L}\frac{\Pi_\eta^R}{\Pi_0^R} - \frac{\Pi_1^R}{\Pi_0^R}\frac{\Pi_\eta^L}{\Pi_0^L}\right)\chi - \frac{3}{2}\frac{\Pi_\eta^L}{\Pi_0^L}\frac{\Pi_\eta^R}{\Pi_0^R}\chi^2\right]$
	Δ_t^η	$(1-\chi)\left(1 + \frac{\Pi_\eta^L}{\Pi_0^L}\chi\right)^{-1}\left(1 + \frac{\Pi_\eta^R}{\Pi_0^R}\chi\right)^{-1}\left[\frac{\Pi_\eta^L}{\Pi_0^L} + \frac{\Pi_\eta^R}{\Pi_0^R} + 2\frac{\Pi_\eta^L}{\Pi_0^L}\frac{\Pi_\eta^R}{\Pi_0^R}\chi\right]\sqrt{\frac{\chi}{1-\chi}}$
NMCHM$_{15_L-15_R}$	$\Delta_t + \delta_t$	$-\left(1 + \frac{\Pi_\eta^L}{\Pi_0^L}\chi\right)^{-1}\left[\frac{\Pi_1^L}{\Pi_0^L} + \frac{\Pi_1^R}{\Pi_0^R} + \frac{3}{2} + \left(\frac{1}{2}\frac{\Pi_\eta^L}{\Pi_0^L} + \frac{\Pi_1^L}{\Pi_0^L}\frac{\Pi_\eta^L}{\Pi_0^R}\right)\chi\right]$
	Δ_t^η	$\left(1 + \frac{\Pi_\eta^L}{\Pi_0^L}\right)\left(1 + \frac{\Pi_\eta^L}{\Pi_0^L}\chi\right)^{-1}\sqrt{\frac{\chi}{1-\chi}}$
NMCHM$_{15_L-20_R}$	$\Delta_t + \delta_t$	$-\left(1 + \frac{\Pi_\eta^L}{\Pi_0^L}\chi\right)^{-1}\left[\frac{\Pi_1^L}{\Pi_0^L} + \frac{\Pi_1^R}{\Pi_0^R} + \frac{3}{2} + \left(\frac{1}{2}\frac{\Pi_\eta^L}{\Pi_0^L} + \frac{\Pi_1^L}{\Pi_0^L}\frac{\Pi_\eta^L}{\Pi_0^R}\right)\chi\right]$
	Δ_t^η	$\left(1 + \frac{\Pi_\eta^L}{\Pi_0^L}\right)\left(1 + \frac{\Pi_\eta^L}{\Pi_0^L}\chi\right)^{-1}\sqrt{\frac{\chi}{1-\chi}}$
NMCHM$_{20_L-1_R}$	$\Delta_t + \delta_t$	$-\left(1 + \frac{\Pi_\eta^L}{\Pi_0^L}\chi\right)^{-1}\left[\frac{\Pi_1^L}{\Pi_0^L} + \frac{3}{2} + \left(\frac{1}{2}\frac{\Pi_\eta^L}{\Pi_0^L} + \frac{\Pi_{h\eta}^L}{\Pi_0^L}\right)\chi\right]$
	Δ_t^η	$\left(1 + \frac{\Pi_\eta^L}{\Pi_0^L}\right)\left(1 + \frac{\Pi_\eta^L}{\Pi_0^L}\chi\right)^{-1}\sqrt{\frac{\chi}{1-\chi}}$
NMCHM$_{20_L-6_R}$	$\Delta_t + \delta_t$	$\left(1 + \frac{\Pi_\eta^L}{\Pi_0^L}\chi\right)^{-1}\left(1 + \frac{\Pi_\eta^R}{\Pi_0^R}\chi\right)^{-1}\left(1 + \frac{\Pi_\eta^{LR}}{\Pi_1^{LR}}\chi\right)^{-1}\left[2\frac{\Pi_2^{LR}}{\Pi_1^{LR}} - \frac{\Pi_1^L}{\Pi_0^L} - \frac{\Pi_1^R}{\Pi_0^R} - \frac{1}{2}\right.$ $+ \left(\frac{1}{2}\frac{\Pi_\eta^L}{\Pi_0^L} + \frac{1}{2}\frac{\Pi_\eta^R}{\Pi_0^R} - \frac{5}{2}\frac{\Pi_\eta^{LR}}{\Pi_1^{LR}} - \frac{\Pi_{h\eta}^L}{\Pi_0^L} + 2\frac{\Pi_2^{LR}}{\Pi_1^{LR}}\frac{\Pi_\eta^L}{\Pi_0^L} + 2\frac{\Pi_2^{LR}}{\Pi_1^{LR}}\frac{\Pi_\eta^R}{\Pi_0^R} - \frac{\Pi_1^L}{\Pi_0^L}\frac{\Pi_\eta^R}{\Pi_0^R}\right.$ $\left. - \frac{\Pi_1^R}{\Pi_0^R}\frac{\Pi_\eta^L}{\Pi_0^L} - \frac{\Pi_1^L}{\Pi_0^L}\frac{\Pi_\eta^{LR}}{\Pi_1^{LR}} - \frac{\Pi_1^R}{\Pi_0^R}\frac{\Pi_\eta^{LR}}{\Pi_1^{LR}}\right)\chi + \left(\frac{3}{2}\frac{\Pi_\eta^L}{\Pi_0^L}\frac{\Pi_\eta^R}{\Pi_0^R} - \frac{3}{2}\frac{\Pi_\eta^L}{\Pi_0^L}\frac{\Pi_\eta^{LR}}{\Pi_1^{LR}} - \frac{3}{2}\frac{\Pi_\eta^R}{\Pi_0^R}\frac{\Pi_\eta^{LR}}{\Pi_1^{LR}}\right.$ $\left. - \frac{\Pi_{h\eta}^L}{\Pi_0^L}\frac{\Pi_\eta^R}{\Pi_0^R} - \frac{\Pi_{h\eta}^L}{\Pi_0^L}\frac{\Pi_\eta^{LR}}{\Pi_1^{LR}} + 2\frac{\Pi_2^{LR}}{\Pi_1^{LR}}\frac{\Pi_\eta^L}{\Pi_0^L}\frac{\Pi_\eta^R}{\Pi_0^R} - \frac{\Pi_1^R}{\Pi_0^R}\frac{\Pi_\eta^L}{\Pi_0^L}\frac{\Pi_\eta^{LR}}{\Pi_1^{LR}} - \frac{\Pi_1^L}{\Pi_0^L}\frac{\Pi_\eta^R}{\Pi_0^R}\frac{\Pi_\eta^{LR}}{\Pi_1^{LR}}\right)\chi^2$ $\left. + \left(-\frac{1}{2}\frac{\Pi_\eta^L}{\Pi_0^L}\frac{\Pi_\eta^R}{\Pi_0^R}\frac{\Pi_\eta^{LR}}{\Pi_1^{LR}} - \frac{\Pi_{h\eta}^L}{\Pi_0^L}\frac{\Pi_\eta^R}{\Pi_0^R}\frac{\Pi_\eta^{LR}}{\Pi_1^{LR}}\right)\chi^3\right]$
	Δ_t^η	$-(1-\chi)\left(1 + \frac{\Pi_\eta^L}{\Pi_0^L}\chi\right)^{-1}\left(1 + \frac{\Pi_\eta^R}{\Pi_0^R}\chi\right)^{-1}\left(1 + \frac{\Pi_\eta^{LR}}{\Pi_1^{LR}}\chi\right)^{-1}$ $\left[2\frac{\Pi_\eta^{LR}}{\Pi_1^{LR}} - \frac{\Pi_\eta^L}{\Pi_0^L} - \frac{\Pi_\eta^R}{\Pi_0^R} + \left(\frac{\Pi_\eta^L}{\Pi_0^L}\frac{\Pi_\eta^{LR}}{\Pi_1^{LR}} + \frac{\Pi_\eta^R}{\Pi_0^R}\frac{\Pi_\eta^{LR}}{\Pi_1^{LR}} - 2\frac{\Pi_\eta^L}{\Pi_0^L}\frac{\Pi_\eta^R}{\Pi_0^R}\right)\chi\right]\sqrt{\frac{\chi}{1-\chi}}$

NMCHM$_{20_\text{L}-15_\text{R}}$	$\Delta_t + \delta_t$	$-\left(1 + \frac{\Pi_\eta^L}{\Pi_0^L}\chi\right)^{-1}\left[\frac{\Pi_1^L}{\Pi_0^L} + \frac{\Pi_1^R}{\Pi_0^R} + \frac{3}{2} + \left(\frac{1}{2}\frac{\Pi_\eta^L}{\Pi_0^L} + \frac{\Pi_{h\eta}^L}{\Pi_0^L} + \frac{\Pi_\eta^L}{\Pi_0^L}\frac{\Pi_1^R}{\Pi_0^R}\right)\chi\right]$
	Δ_t^η	$\left(1 + \frac{\Pi_\eta^L}{\Pi_0^L}\right)\left(1 + \frac{\Pi_\eta^L}{\Pi_0^L}\chi\right)^{-1}\sqrt{\frac{\chi}{1-\chi}}$
NMCHM$_{20_\text{L}-20_\text{R}}$	$\Delta_t + \delta_t$	$\left(1 + \frac{\Pi_\eta^L}{\Pi_0^L}\chi\right)^{-1}\left[2\frac{\Pi_2^{LR}}{\Pi_1^{LR}} - \frac{\Pi_1^L}{\Pi_0^L} - \frac{\Pi_1^R}{\Pi_0^R} - \frac{3}{2}\right.$ $\left. + \left(2\frac{\Pi_2^{LR}}{\Pi_1^{LR}}\frac{\Pi_\eta^L}{\Pi_0^L} - \frac{\Pi_1^R}{\Pi_0^R}\frac{\Pi_\eta^L}{\Pi_0^L} - \frac{1}{2}\frac{\Pi_\eta^L}{\Pi_0^L} - \frac{\Pi_{h\eta}^L}{\Pi_0^L}\right)\chi\right]$
	Δ_t^η	$\left(1 + \frac{\Pi_\eta^L}{\Pi_0^L}\right)\left(1 + \frac{\Pi_\eta^L}{\Pi_0^L}\chi\right)^{-1}\sqrt{\frac{\chi}{1-\chi}}$

Table 6. Expressions for $(\Delta_t + \delta_t)$ and Δ_t^η for different representations of SO(6) in which the top quark is embedded.

References

[1] D.B. Kaplan and H. Georgi, SU(2) × U(1) *Breaking by Vacuum Misalignment*, *Phys. Lett.* **B 136** (1984) 183 [INSPIRE].

[2] M.J. Dugan, H. Georgi and D.B. Kaplan, *Anatomy of a Composite Higgs Model*, *Nucl. Phys.* **B 254** (1985) 299 [INSPIRE].

[3] R. Contino, *The Higgs as a Composite Nambu-Goldstone Boson*, in *Physics of the large and the small, TASI 09, proceedings of the Theoretical Advanced Study Institute in Elementary Particle Physics*, Boulder, Colorado, U.S.A., 1–26 June 2009, pp. 235–306 (2011) DOI:10.1142/9789814327183_0005 [arXiv:1005.4269] [INSPIRE].

[4] G. Panico and A. Wulzer, *The Composite Nambu-Goldstone Higgs*, *Lect. Notes Phys.* **913** (2016) pp.1 [arXiv:1506.01961] [INSPIRE].

[5] C. Csáki and P. Tanedo, *Beyond the Standard Model*, in *Proceedings, 2013 European School of High-Energy Physics (ESHEP 2013)*, Paradfurdo, Hungary, June 5–18, 2013, pp. 169–268 (2015) DOI:10.5170/CERN-2015-004.169 [arXiv:1602.04228] [INSPIRE].

[6] R. Contino, Y. Nomura and A. Pomarol, *Higgs as a holographic pseudoGoldstone boson*, *Nucl. Phys.* **B 671** (2003) 148 [hep-ph/0306259] [INSPIRE].

[7] R. Contino, T. Kramer, M. Son and R. Sundrum, *Warped/composite phenomenology simplified*, *JHEP* **05** (2007) 074 [hep-ph/0612180] [INSPIRE].

[8] C. Csáki, M. Geller and O. Telem, *Tree-level Quartic for a Holographic Composite Higgs*, arXiv:1710.08921 [INSPIRE].

[9] D. Espriu and A. Katanaeva, *Holographic description of* SO(5) → SO(4) *composite Higgs model*, arXiv:1706.02651 [INSPIRE].

[10] A. De Simone, O. Matsedonskyi, R. Rattazzi and A. Wulzer, *A First Top Partner Hunter's Guide*, *JHEP* **04** (2013) 004 [arXiv:1211.5663] [INSPIRE].

[11] A. Thamm, R. Torre and A. Wulzer, *Future tests of Higgs compositeness: direct vs indirect*, *JHEP* **07** (2015) 100 [arXiv:1502.01701] [inSPIRE].

[12] A. Azatov, D. Chowdhury, D. Ghosh and T.S. Ray, *Same sign di-lepton candles of the composite gluons*, *JHEP* **08** (2015) 140 [arXiv:1505.01506] [inSPIRE].

[13] J.P. Araque, N.F. Castro and J. Santiago, *Interpretation of Vector-like Quark Searches: Heavy Gluons in Composite Higgs Models*, *JHEP* **11** (2015) 120 [arXiv:1507.05628] [inSPIRE].

[14] ATLAS collaboration, *Search for pair production of vector-like top quarks in events with one lepton, jets and missing transverse momentum in $\sqrt{s} = 13\,TeV$ pp collisions with the ATLAS detector*, *JHEP* **08** (2017) 052 [arXiv:1705.10751] [inSPIRE].

[15] CMS collaboration, *Search for top quark partners with charge 5/3 in proton-proton collisions at $\sqrt{s} = 13\,TeV$*, *JHEP* **08** (2017) 073 [arXiv:1705.10967] [inSPIRE].

[16] CMS collaboration, *Search for pair production of vector-like T and B quarks in single-lepton final states using boosted jet substructure in proton-proton collisions at $\sqrt{s} = 13\,TeV$*, *JHEP* **11** (2017) 085 [arXiv:1706.03408] [inSPIRE].

[17] M. Chala, *Direct bounds on heavy toplike quarks with standard and exotic decays*, *Phys. Rev.* **D 96** (2017) 015028 [arXiv:1705.03013] [inSPIRE].

[18] J. Yepes and A. Zerwekh, *Top partner-resonance interplay in a composite Higgs framework*, arXiv:1711.10523 [inSPIRE].

[19] D. Pappadopulo, A. Thamm and R. Torre, *A minimally tuned composite Higgs model from an extra dimension*, *JHEP* **07** (2013) 058 [arXiv:1303.3062] [inSPIRE].

[20] D. Croon, B.M. Dillon, S.J. Huber and V. Sanz, *Exploring holographic Composite Higgs models*, *JHEP* **07** (2016) 072 [arXiv:1510.08482] [inSPIRE].

[21] A. Banerjee, G. Bhattacharyya and T.S. Ray, *Improving Fine-tuning in Composite Higgs Models*, *Phys. Rev.* **D 96** (2017) 035040 [arXiv:1703.08011] [inSPIRE].

[22] C. Csáki, T. Ma and J. Shu, *Trigonometric Parity for the Composite Higgs*, arXiv:1709.08636 [inSPIRE].

[23] Z. Chacko, H.-S. Goh and R. Harnik, *The Twin Higgs: Natural electroweak breaking from mirror symmetry*, *Phys. Rev. Lett.* **96** (2006) 231802 [hep-ph/0506256] [inSPIRE].

[24] K. Agashe, R. Contino and A. Pomarol, *The Minimal composite Higgs model*, *Nucl. Phys.* **B 719** (2005) 165 [hep-ph/0412089] [inSPIRE].

[25] G. Panico and A. Wulzer, *The Discrete Composite Higgs Model*, *JHEP* **09** (2011) 135 [arXiv:1106.2719] [inSPIRE].

[26] O. Matsedonskyi, G. Panico and A. Wulzer, *Light Top Partners for a Light Composite Higgs*, *JHEP* **01** (2013) 164 [arXiv:1204.6333] [inSPIRE].

[27] D. Marzocca, M. Serone and J. Shu, *General Composite Higgs Models*, *JHEP* **08** (2012) 013 [arXiv:1205.0770] [inSPIRE].

[28] A. Pomarol and F. Riva, *The Composite Higgs and Light Resonance Connection*, *JHEP* **08** (2012) 135 [arXiv:1205.6434] [inSPIRE].

[29] M. Carena, L. Da Rold and E. Pontón, *Minimal Composite Higgs Models at the LHC*, *JHEP* **06** (2014) 159 [arXiv:1402.2987] [inSPIRE].

[30] G. Panico, M. Redi, A. Tesi and A. Wulzer, *On the Tuning and the Mass of the Composite Higgs*, *JHEP* **03** (2013) 051 [`arXiv:1210.7114`] [ɪɴSPIRE].

[31] M. Montull, F. Riva, E. Salvioni and R. Torre, *Higgs Couplings in Composite Models*, *Phys. Rev.* **D 88** (2013) 095006 [`arXiv:1308.0559`] [ɪɴSPIRE].

[32] A. Carmona and F. Goertz, *A naturally light Higgs without light Top Partners*, *JHEP* **05** (2015) 002 [`arXiv:1410.8555`] [ɪɴSPIRE].

[33] S. Kanemura, K. Kaneta, N. Machida, S. Odori and T. Shindou, *Single and double production of the Higgs boson at hadron and lepton colliders in minimal composite Higgs models*, *Phys. Rev.* **D 94** (2016) 015028 [`arXiv:1603.05588`] [ɪɴSPIRE].

[34] M.B. Gavela, K. Kanshin, P.A.N. Machado and S. Saa, *The linear-non-linear frontier for the Goldstone Higgs*, *Eur. Phys. J.* **C 76** (2016) 690 [`arXiv:1610.08083`] [ɪɴSPIRE].

[35] D. Liu, I. Low and C.E.M. Wagner, *Modification of Higgs Couplings in Minimal Composite Models*, *Phys. Rev.* **D 96** (2017) 035013 [`arXiv:1703.07791`] [ɪɴSPIRE].

[36] B. Gripaios, A. Pomarol, F. Riva and J. Serra, *Beyond the Minimal Composite Higgs Model*, *JHEP* **04** (2009) 070 [`arXiv:0902.1483`] [ɪɴSPIRE].

[37] M. Redi and A. Tesi, *Implications of a Light Higgs in Composite Models*, *JHEP* **10** (2012) 166 [`arXiv:1205.0232`] [ɪɴSPIRE].

[38] J. Barnard, T. Gherghetta and T.S. Ray, *UV descriptions of composite Higgs models without elementary scalars*, *JHEP* **02** (2014) 002 [`arXiv:1311.6562`] [ɪɴSPIRE].

[39] J. Serra, *Beyond the Minimal Top Partner Decay*, *JHEP* **09** (2015) 176 [`arXiv:1506.05110`] [ɪɴSPIRE].

[40] M. Low, A. Tesi and L.-T. Wang, *A pseudoscalar decaying to photon pairs in the early LHC Run 2 data*, *JHEP* **03** (2016) 108 [`arXiv:1512.05328`] [ɪɴSPIRE].

[41] H. Cai, T. Flacke and M. Lespinasse, *A composite scalar hint from di-boson resonances?*, `arXiv:1512.04508` [ɪɴSPIRE].

[42] A. Arbey, G. Cacciapaglia, H. Cai, A. Deandrea, S. Le Corre and F. Sannino, *Fundamental Composite Electroweak Dynamics: Status at the LHC*, *Phys. Rev.* **D 95** (2017) 015028 [`arXiv:1502.04718`] [ɪɴSPIRE].

[43] C. Niehoff, P. Stangl and D.M. Straub, *Electroweak symmetry breaking and collider signatures in the next-to-minimal composite Higgs model*, *JHEP* **04** (2017) 117 [`arXiv:1611.09356`] [ɪɴSPIRE].

[44] V. Sanz and J. Setford, *Composite Higgs models after Run2*, `arXiv:1703.10190` [ɪɴSPIRE].

[45] G.F. Giudice, C. Grojean, A. Pomarol and R. Rattazzi, *The Strongly-Interacting Light Higgs*, *JHEP* **06** (2007) 045 [`hep-ph/0703164`] [ɪɴSPIRE].

[46] R. Contino, M. Ghezzi, C. Grojean, M. Muhlleitner and M. Spira, *Effective Lagrangian for a light Higgs-like scalar*, *JHEP* **07** (2013) 035 [`arXiv:1303.3876`] [ɪɴSPIRE].

[47] M. Hashimoto, *Revisiting vectorlike quark models with enhanced top Yukawa coupling*, *Phys. Rev.* **D 96** (2017) 035020 [`arXiv:1704.02615`] [ɪɴSPIRE].

[48] S. Jana and S. Nandi, *New Physics Scale from Higgs Observables with Effective Dimension-6 Operators*, `arXiv:1710.00619` [ɪɴSPIRE].

[49] G. Cacciapaglia, A. Deandrea, G. Drieu La Rochelle and J.-B. Flament, *Higgs couplings beyond the Standard Model*, *JHEP* **03** (2013) 029 [arXiv:1210.8120] [ɪɴSPIRE].

[50] A. Falkowski, F. Riva and A. Urbano, *Higgs at last*, *JHEP* **11** (2013) 111 [arXiv:1303.1812] [ɪɴSPIRE].

[51] A. Azatov, R. Contino, A. Di Iura and J. Galloway, *New Prospects for Higgs Compositeness in $h \to Z\gamma$*, *Phys. Rev.* **D 88** (2013) 075019 [arXiv:1308.2676] [ɪɴSPIRE].

[52] S.R. Coleman and E.J. Weinberg, *Radiative Corrections as the Origin of Spontaneous Symmetry Breaking*, *Phys. Rev.* **D 7** (1973) 1888 [ɪɴSPIRE].

[53] ATLAS, CMS collaborations, *Measurements of the Higgs boson production and decay rates and constraints on its couplings from a combined ATLAS and CMS analysis of the LHC pp collision data at $\sqrt{s} = 7$ and $8\,TeV$*, *JHEP* **08** (2016) 045 [arXiv:1606.02266] [ɪɴSPIRE].

[54] ATLAS collaboration, *Measurements of the Higgs boson production cross section via Vector Boson Fusion and associated WH production in the $WW^* \to \ell\nu\ell\nu$ decay mode with the ATLAS detector at $\sqrt{s} = 13\,TeV$*, ATLAS-CONF-2016-112 (2016).

[55] ATLAS collaboration, *Measurements of Higgs boson properties in the diphoton decay channel with $36.1\,fb^{-1}$ pp collision data at the center-of-mass energy of $13\,TeV$ with the ATLAS detector*, ATLAS-CONF-2017-045 (2017).

[56] ATLAS collaboration, *Evidence for the associated production of the Higgs boson and a top quark pair with the ATLAS detector*, ATLAS-CONF-2017-077 (2017).

[57] ATLAS collaboration, *Measurement of the Higgs boson coupling properties in the $H \to ZZ^* \to 4\ell$ decay channel at $\sqrt{s} = 13\,TeV$ with the ATLAS detector*, ATLAS-CONF-2017-043 (2017).

[58] ATLAS collaboration, *Evidence for the $H \to b\bar{b}$ decay with the ATLAS detector*, *JHEP* **12** (2017) 024 [arXiv:1708.03299] [ɪɴSPIRE].

[59] ATLAS collaboration, *Search for the Standard Model Higgs boson produced in association with top quarks and decaying into a $b\bar{b}$ pair in pp collisions at $\sqrt{s} = 13\,TeV$ with the ATLAS detector*, ATLAS-CONF-2017-076 (2017).

[60] CMS collaboration, *Higgs to WW measurements with $15.2\,fb^{-1}$ of $13\,TeV$ proton-proton collisions*, CMS-PAS-HIG-16-021.

[61] CMS collaboration, *Measurements of properties of the Higgs boson in the diphoton decay channel with the full 2016 data set*, CMS-PAS-HIG-16-040.

[62] CMS collaboration, *Measurements of properties of the Higgs boson decaying into the four-lepton final state in pp collisions at $\sqrt{s} = 13\,TeV$*, *JHEP* **11** (2017) 047 [arXiv:1706.09936] [ɪɴSPIRE].

[63] CMS collaboration, *Observation of the Higgs boson decay to a pair of τ leptons with the CMS detector*, *Phys. Lett.* **B 779** (2018) 283 [arXiv:1708.00373] [ɪɴSPIRE].

[64] CMS collaboration, *Evidence for the Higgs boson decay to a bottom quark-antiquark pair*, arXiv:1709.07497 [ɪɴSPIRE].

[65] CMS collaboration, *Search for the associated production of a Higgs boson with a top quark pair in final states with a τ lepton at $\sqrt{s} = 13$ TeV*, CMS-PAS-HIG-17-003.

[66] CMS collaboration, *Search for Higgs boson production in association with top quarks in multilepton final states at $\sqrt{s} = 13$ TeV*, CMS-PAS-HIG-17-004.

[67] A. Azatov and J. Galloway, *Light Custodians and Higgs Physics in Composite Models*, *Phys. Rev.* **D 85** (2012) 055013 [`arXiv:1110.5646`] [ɪɴSPIRE].

[68] M. Frigerio, J. Serra and A. Varagnolo, *Composite GUTs: models and expectations at the LHC*, *JHEP* **06** (2011) 029 [`arXiv:1103.2997`] [ɪɴSPIRE].

[69] J. Barnard, T. Gherghetta, T.S. Ray and A. Spray, *The Unnatural Composite Higgs*, *JHEP* **01** (2015) 067 [`arXiv:1409.7391`] [ɪɴSPIRE].

[70] M. Frigerio, A. Pomarol, F. Riva and A. Urbano, *Composite Scalar Dark Matter*, *JHEP* **07** (2012) 015 [`arXiv:1204.2808`] [ɪɴSPIRE].

[71] D. Marzocca and A. Urbano, *Composite Dark Matter and LHC Interplay*, *JHEP* **07** (2014) 107 [`arXiv:1404.7419`] [ɪɴSPIRE].

[72] N. Fonseca, R. Zukanovich Funchal, A. Lessa and L. Lopez-Honorez, *Dark Matter Constraints on Composite Higgs Models*, *JHEP* **06** (2015) 154 [`arXiv:1501.05957`] [ɪɴSPIRE].

[73] M. Kim, S.J. Lee and A. Parolini, *WIMP Dark Matter in Composite Higgs Models and the Dilaton Portal*, `arXiv:1602.05590` [ɪɴSPIRE].

[74] J. Ellis and T. You, *Global Analysis of Experimental Constraints on a Possible Higgs-Like Particle with Mass 125 GeV*, *JHEP* **06** (2012) 140 [`arXiv:1204.0464`] [ɪɴSPIRE].

[75] M. Chala, G. Durieux, C. Grojean, L. de Lima and O. Matsedonskyi, *Minimally extended SILH*, *JHEP* **06** (2017) 088 [`arXiv:1703.10624`] [ɪɴSPIRE].